metals

MDPI

Article

Effect of Nb Alloying and Solution Treatment on the Mechanical Properties of Cold-Rolled Fe-Mn-Al-C Low-Density Steel

Litu Huo, Jianxin Gao, Yungang Li, Pengfei Xu, Xiangyu Wei and Tao Ma *

College of Metallurgy and Energy, North China University of Science and Technology, Tangshan 063210, China; hlt_8df08@163.com (L.H.); gjx@ncst.edu.cn (J.G.); lyg@ncst.edu.cn (Y.L.); 17330216397@163.com (P.X.); weixiangyu1015@163.com (X.W.)

* Correspondence: matao@ncst.edu.cn

Abstract: The automotive industry's rapid expansion has made the development of lightweight, high-strength automotive steels essential for both energy efficiency and emission reduction. Among these materials, Fe-Mn-Al-C steel has drawn considerable interest due to its favorable combination of low density and high strength. This research examines the impact of Nb alloying (with Nb content of 0% and 0.5%) and solution treatment on the microstructure and mechanical properties of cold-rolled Fe-28Mn-10Al-C low-density steel. Various methods were employed, including Thermo-Calc thermodynamic simulations, the Olson–Cohen model, X-ray diffraction (XRD), metallographic microscopy, room-temperature tensile testing, and scanning electron microscopy (SEM). The findings demonstrate that Nb alloying significantly refines the austenite grain structure of the Fe-28Mn-10Al-C steel, improving both strength and ductility in comparison to the 0Nb steel. After solution treatment at 1050 °C for 30 min, the cold-rolling-induced defects are effectively removed, leading to a substantial increase in elongation at fracture (38.14–44.45%) and an ultimate tensile strength exceeding 900 MPa. As the solution treatment temperature increases, the austenite grains coarsen, and the number of twins increases, while yield strength and ultimate tensile strength decrease. However, there is a notable enhancement in ductility, with the material exhibiting a ductile fracture mechanism. These results offer valuable insights and a theoretical foundation for further improving the mechanical properties of Fe-Mn-Al-C low-density steels.

Keywords: Fe-Mn-Al-C; Nb; microstructure; thermodynamics; SFE; mechanical properties

check for updates

Academic Editors: Frank Czerwinski and Koh-ichi Sugimoto

Received: 16 December 2024
Revised: 18 January 2025
Accepted: 18 January 2025
Published: 22 January 2025

Citation: Huo, L.; Gao, J.; Li, Y.; Xu, P.; Wei, X.; Ma, T. Effect of Nb Alloying and Solution Treatment on the Mechanical Properties of Cold-Rolled Fe-Mn-Al-C Low-Density Steel. *Metals* **2025**, *15*, 102. https://doi.org/10.3390/met15020102

Copyright: © 2025 by the authors. Licensee MDPI, Basel, Switzerland. This article is an open access article distributed under the terms and conditions of the Creative Commons Attribution (CC BY) license (https://creativecommons.org/licenses/by/4.0/).

1. Introduction

In recent years, the rapid development of the automotive industry has brought increasing attention to issues such as energy consumption and exhaust emissions. Data suggest that optimizing vehicle structural design and developing lightweight, high-strength automotive steels are essential for improving fuel efficiency and reducing pollutant emissions. Fe-Mn-Al-C steel, first developed in the 1950s, is known for its excellent mechanical properties and low density, offering significant potential for use in automotive structural materials [1–3]. Among these, reducing overall vehicle weight using lightweight materials has become an effective strategy and is widely favored by researchers [4,5].

Studies have shown that Fe-Mn-Al-C steel alloyed with Mn and Al exhibits characteristics such as low density [6–8], high strength, and excellent weldability, making it promising for a wide range of automotive structural applications [9,10]. The phase composition and precipitate phases of Fe-Mn-Al-C low-density steel are significantly influenced by processing and heat treatment conditions, which in turn affect the overall properties of the

material. Pang et al. [11] investigated the mechanical properties of Fe-22.8Mn-8.48Al-0.86C low-density steel after solution treatment at 1100 °C for 1 h. The results showed that the solid solution treatment resulted in an austenitic organization with twinned crystals, leading to a tensile strength of 757.4 MPa and a total elongation of 68%. Liu et al. [12] found that after heat treatment at 1000 °C, the microstructure of the steel consisted of a single-phase austenite. Reducing the annealing temperature to 900 °C led to a eutectoid reaction, producing a mixed phase of ferrite and κ-carbide, with nanoscale κ-carbides precipitating at grain boundaries. At 800 °C, a lamellar mixture of κ-carbide and ferrite was formed. Further research [13] indicated that sub-micron κ-carbides at grain boundaries obtained after cold rolling and solution treatment hinder dislocation movement, thus enhancing the strain hardening capacity of the material. Zheng et al. [14] observed that with prolonged solution treatment, the number of recrystallized grains increased, dislocation density decreased, and the microstructure evolved from a uniform distribution to a cubic weave. In the early stages of recrystallization, dislocation walls formed by dislocation slip hinder dislocation motion, thereby improving the tensile strength of the material. Therefore, optimizing heat treatment parameters can effectively control the phase composition, precipitate phases, and substructural characteristics in Fe-Mn-Al-C low-density steel, achieving the desired high strength and plasticity.

In addition to regulating heat treatment process parameters, microalloying is increasingly applied in the development of high-performance steel materials [15–17]. Research has shown that Nb alloying plays a significant role in controlling the microstructural and mechanical properties of steel. As a strong carbide-forming element, Nb, when added to steel, can form highly stable carbides by either dissolving or combining with carbon in the steel. During high-temperature treatment or deformation, undissolved NbC precipitates act as pinning agents at grain boundaries and dislocations, inhibiting the growth of austenite grains and the movement of dislocations, thereby enhancing the material strength and toughness through grain refinement and precipitation strengthening [18]. As a typical alloying element, Nb has been widely used in the development of heat-resistant steels, hot-formed steels, and stainless steels in recent years [19]. Significant progress has been made internationally in studying the effects of Nb on the microstructure, mechanical properties, and wear resistance of automotive steels [20,21]. For example, Huo et al. [22] found that increasing the Nb content from 0.02 wt% to 0.1 wt% in Fe-4Mn-2Al-0.2C steel resulted in a grain refinement strengthening effect of 50–100 MPa, but Nb also promoted carbide precipitation, delayed recrystallization, and reduced the stability of austenite in the steel. Considering solid-solution strengthening factors, high-manganese steels exhibited superior mechanical properties compared to medium- and low-manganese steels. Zhao [23] found that Fe-28Mn-7Al-C steel microalloyed with Nb-V (concentration of 0.16 wt% each) achieved a high tensile strength of 940 MPa, an increase of 379 MPa over the unalloyed original steel, due to the effects of grain refinement and precipitation strengthening. Li et al. [24] investigated the effects of co-addition of 0.51Ti-0.34Mo-0.075Nb on the microstructure and tensile behavior of austenitic Fe–26Mn–8Al-1.5C steel aged at 500–600 °C and found that Ti–Mo–Nb microalloying refined the austenite grains, increased the size and volume fraction of κ-carbides, and formed (Ti, Mo, Nb)C particles at both the grain boundaries and within grains, thereby achieving higher yield strength. Currently, few systematic studies have been conducted on the microstructural evolution of high-manganese, high-aluminum Fe-Mn-Al-C steel with Nb, and further exploration is needed on the structural and mechanical properties of Fe-Mn-Al-C-Nb steel with higher Nb content (greater than 0.1%). This study focuses on high-manganese, high-aluminum, low-density Fe-28Mn-10Al-C steel, analyzing the effects of Nb addition on the microstructural evolution of high-manganese, high-aluminum steel based on thermodynamic calculations to determine the appropriate

Nb content for the experimental steel. The steel containing Nb was subjected to different solution treatment processes after cold rolling to investigate the impact and mechanisms of Nb content and solution temperature on the microstructural evolution and mechanical properties of low-density steel.

2. Materials and Methods

Using high-manganese Fe-28Mn-10Al-C steel as the base composition, Therm-Calc (Version 2019a, TCFE8.) thermodynamic software was employed to investigate the effects of Nb addition on the microstructure and decomposition reactions of Fe-Mn-Al-C low-density steel. The equilibrium state of Nb in the steel was calculated, and the alloy composition was designed and optimized.

Based on thermodynamic calculations, Fe-28Mn-10Al-C-xNb alloys were prepared by adding Nb elements (with mass fractions of 0 and 0.5%) during the melting process. Initially, 25 kg ingots were melted in an induction furnace (KJ-M1200-12LZ, Zhengzhou Kejia Electric Furnace Co., Zhengzhou, China) under an argon atmosphere, followed by forging into billets with an 80 mm × 40 mm cross section after holding at 1150 °C for 2 h. The billets were then hot-rolled to a thickness of 5mm after homogenization at 1200 °C for 2 h. The hot-rolled plates were solution treated at 1150 °C for 1 h and quenched in water to room temperature. After pickling to remove the oxide layer, the steel plates were cold-rolled at room temperature through a four-high rolling mill (Φ85/Φ350 × 450 four-roll cold rolling mill, Wuxi Xingxiang Metallurgical machinery Co., Ltd., Wuxi, China) in 10 passes, achieving a reduction rate of 66% to produce thin sheets with a thickness of 1.7 mm. The cold-rolled sheets were then subjected to high-temperature solution treatment at 950 °C, 1000 °C, and 1050 °C for 30 min, followed by cooling to room temperature at a rate of 120 °C/s. The treated samples were sequentially ground with 320#, 500#, 800#, 1200#, and 2000#, mechanically polished, and then etched with a 4% nitric acid alcohol solution. After rinsing thoroughly with water and wiping with alcohol, the austenite grain morphology was observed under a Zeiss metallographic microscope (Axiovert 200MAT, Carl Zeiss AG, Jena, Germany). Microstructural characterization was carried out using a Quanta 650 scanning electron microscope (SEM, FEI Quanta 650, Thermo Fisher Scientific, Hillsboro, OR, USA). Tensile test specimens were prepared from the solution-treated, cold-rolled plates in the rolling direction and mechanically tested. Tensile tests were conducted at room temperature on an INSTRON 3382 universal testing machine (INSTRON 3382, Instron, Norwood, MA, USA) with an initial strain rate of 1×10^{-3} s^{-1} and a constant pulling speed of 3 mm/min until sample fracture. Phase analysis was performed using a D/Max/PC type X-ray diffractometer ((XRD, Rigaku, D/Max/PC, RigakuCorporation, Tokyo, Japan) with Cu target radiation, a diffraction angle range of 40–100°, a scanning speed of 5 °/min, and a step size of 0.020°.

3. Results

3.1. Thermodynamic Calculation of the Influence of Nb on the Phase Transition and Precipitation Behavior of Fe-28Mn-10Al-C Steel

Figure 1 presents the equilibrium phase diagrams of Fe-28Mn-10Al-C-xNb low-density steels with varying Nb contents (all mass fractions are provided in the text), calculated using Thermo-Calc thermodynamic software within the temperature range of 200–1600 °C. As shown in Figure 1, Fe-Mn-Al-C low-density steels with different Nb concentrations exhibit various phases, including liquid phase (L), austenite (γ), low-temperature ferrite (α), κ-carbide (κ), and M23C6 carbide, under different temperature conditions. At higher Mn and Al contents, the low-density steel begins to precipitate austenite from the liquid phase at approximately 1200 °C, maintaining a stable two-phase region between 800 °C and

1200 °C. As the temperature decreases, the austenite undergoes eutectic transformation, precipitating α-ferrite and κ-carbides, which leads to a reduction in the volume fraction of austenite. Figure 1 also shows that the precipitation temperatures of α-ferrite and κ-phase in low-density steel are not significantly affected by the increase in Nb concentration, although their contents gradually decrease with increasing Nb content. Table 1 presents the limiting contents of κ-carbide (ωκ-carbide) and low-temperature α-ferrite (ωα-ferrite) in Fe-28Mn-10Al-C-xNb low-density steels at various Nb concentrations (ωNb). As shown in Table 1, when the Nb content increases from 0% to 0.5%, the limiting content of κ-carbide in Fe-28Mn-10Al-C-xNb low-density steel decreases from 13.87% to 13.71%, while the α-ferrite content decreases from 86.28% to 85.77%. Under equilibrium conditions, the addition of Nb can effectively suppress the decomposition and eutectoid transformation of austenite in Fe-28Mn-10Al-C low-density steel, thereby reducing the concentrations of α-ferrite and κ-carbide.

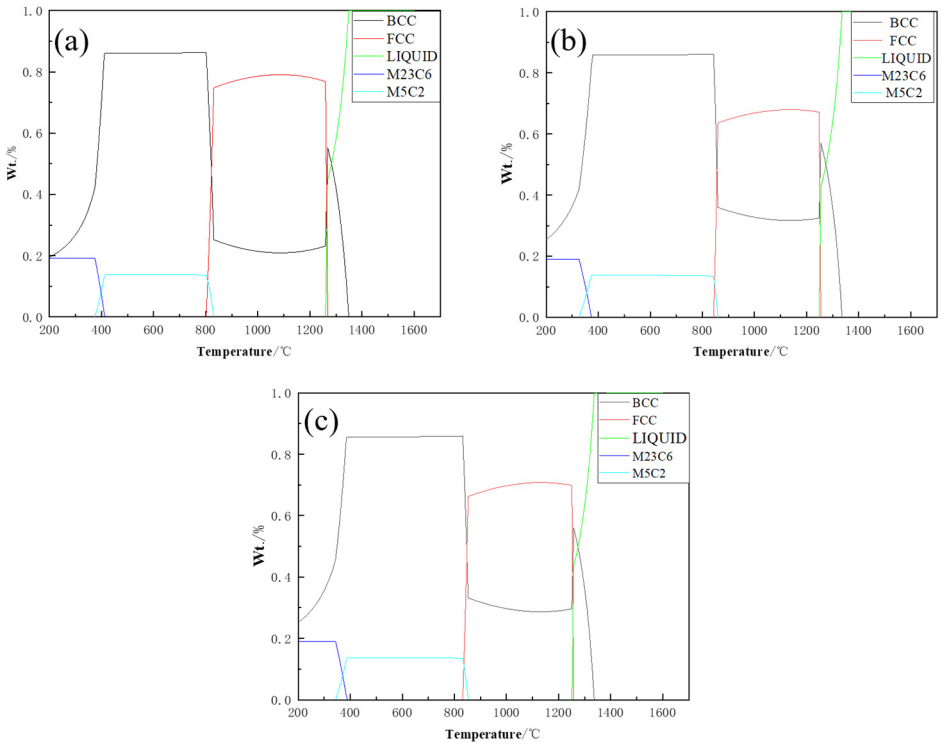


Figure 1. Phase diagram of Fe-28Mn-10Al-098C-xNb low-density steel calculated using Thermo-Calc: (**a**) Fe-28Mn-10Al-C, (**b**) Fe-28Mn-10Al-C-0.3Nb, (**c**) Fe-28Mn-10Al-C-0.5Nb.

Table 1. Ultimate content of κ-carbide and low-temperature α-ferrite in Fe-28Mn-10Al-C low-density steel at different Nb contents.

ω_{Nb}/%	$\omega_{\kappa\text{-carbide}}$/%	$\omega_{\alpha\text{-ferrite}}$/%
0	13.87	86.28
0.3	13.75	85.86
0.5	13.71	85.77

Under equilibrium conditions, the mass fraction of NbC in 0.3 and 0.5Nb steels varies with temperature, as shown in Figure 2. The complete solid solution temperatures for NbC are 1340 °C and 1400 °C, respectively. As the temperature increases, NbC continues to dissolve, and its mass fraction decreases rapidly. At 850 °C, the limiting mass fractions of NbC in the two experimental steels are 0.00403 and 0.00595, respectively. Nearly all the Nb

elements added to the steel will exist in the form of a precipitated phase, as indicated by thermodynamic calculations.

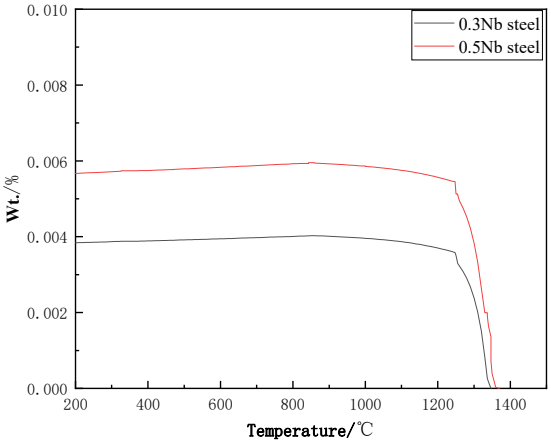


Figure 2. Localized magnification of NbC precipitation phases in Fe-28Mn-10Al-C-xNb low-density steels with different Nb contents.

Thermodynamic calculations indicate that Fe-28Mn-10Al-C-xNb low-density steel can achieve an austenitic structure within the temperature range of 800–1200 °C under the designed compositional conditions. Rapid cooling after heat treatment in this temperature range can stabilize austenite at room temperature, thereby enhancing the mechanical properties of the steel. In the equilibrium state, when the temperature drops below 800 °C, κ-carbide precipitation occurs in the steel. The morphology and distribution of κ-carbides influence their precipitation strengthening effect in low-density steel. Previous studies have shown that the diffuse distribution of nanoscale κ-carbides at grain boundaries and within grains impedes dislocation motion, which improves matrix strength. However, the lamellar aggregation and continuous distribution of κ-carbides at grain boundaries lead to increased hardness, which significantly reduces ductility and increases the risk of brittle fracture [25–27]. Therefore, minimizing κ-carbide formation during the heat treatment process is crucial. Based on this, the solid solution heat treatment temperatures were set above 900 °C.

In addition, according to the theory of second-phase solid solution in steel, the solubility of niobium (Nb) in steel is extremely low. The degree of Nb solid solution is influenced by the carbon (C) content in the steel and the heat treatment temperature. Under high-temperature conditions, the degree of solid solution of Nb in austenite can generally be expressed as follows [28,29]:

$$\lg\left(C_C \cdot C_{Nb}^{0.875}\right) = 2.97 - 7500/T \pm 0.06 \quad (1)$$

In the equation:

C_C—carbon content in steel, %;
C_{Nb}—niobium (Nb) solubility in steel, %;
T—heat treatment temperature, K.

From Equation (1), it can be observed that at 950 °C (1223 K), 1000 °C (1273 K), and 1050 °C (1323 K), the niobium (Nb) exhibits a solid solubility of only 0.0002%, 0.00039%, and 0.0007% in austenite, respectively. Furthermore, thermodynamic calculations suggest that Nb addition suppresses the decomposition of austenite and the precipitation of κ-carbides in Fe-28Mn-10Al-C steel, thus stabilizing the austenitic structure. Under the designed alloy composition, Nb primarily exists as precipitate-phase precipitates in

the low-density steel. At the same time, based on our investigation of the composition, size, morphology, and distribution of precipitates in steels with identical compositions (as shown in Figure 3) [30], the precipitates in low-density Fe-Mn-Al-C-Nb steel are finely dispersed along the austenite grain boundaries, with an average size of approximately 450 nm. Energy-dispersive X-ray spectroscopy (EDS) analysis identified the precipitates as NbC. Selected area diffraction pattern (SADP) results revealed distinct "satellite spots" around the main diffraction points, indicating the formation of ordered phases resembling austenite in the microstructure after amplitude modulation decomposition. Concurrently, the lattice constant also exhibits corresponding changes. At low Nb concentrations, the inhibition of austenite decomposition is reduced, resulting in less precipitate phase. This, in turn, weakens second-phase strengthening and grain refinement. As Nb content increases, its low solubility in austenite promotes the formation of a coarse, micron-sized precipitate phase. Due to the high melting point of NbC (3600 °C) and its strong stability, these particles are difficult to eliminate, even with high-temperature solid solution treatment. Furthermore, the presence of coarse precipitate-phase particles tends to concentrate stress during deformation, negatively impacting toughness, plasticity, and overall material performance. Based on the calculation results, two alloys were prepared by melting, with the chemical compositions of the experimental steels measured by chemical analysis, as shown in Table 2, denoted as 0Nb and 0.5Nb steel. The densities of the two steels were measured using a Byes-300A density meter (Bon Yi Precision Measuring Instrument (Shanghai) Co., LTD., Shanghai, China) and found to be 6.30 g/cm^3 and 6.29 g/cm^3, respectively, representing reductions of 19.8% and 20.0% compared to pure iron. This reduction can be primarily attributed to the higher Al content in the 0.5Nb steel, with the minor addition of Nb having a negligible effect on the density. Therefore, the density of the steel is mainly influenced by its Al content.

Table 2. Chemical composition of Fe-Mn-Al-C-Nb steels (mass percent, %).

Steel	w_C/%	w_{Mn}/%	w_{Al}/%	w_{Nb}/%	w_S/%	w_N/%	w_P/%	w_{Fe}/%
0Nb	0.98	28.53	10.21	—	≤0.003	0.0056	≤0.003	Bal.
0.5Nb	1.05	29.82	10.95	0.56	≤0.003	0.0041	≤0.003	Bal.

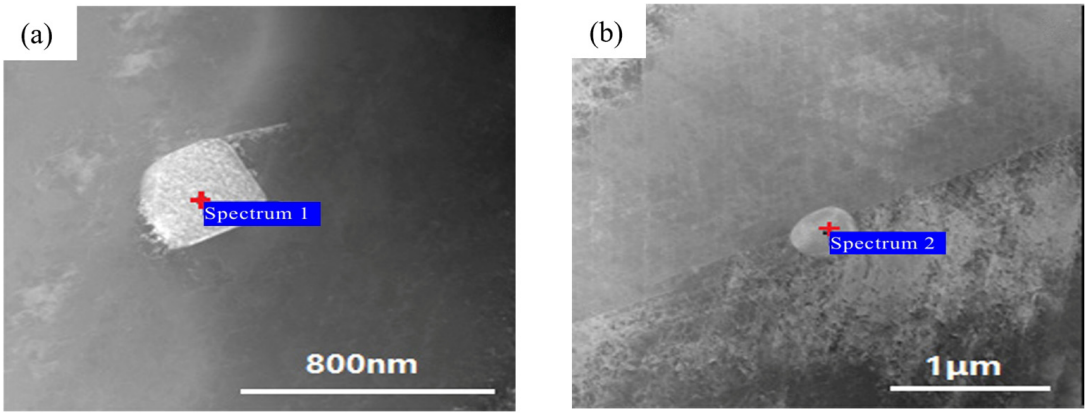


Figure 3. *Cont.*

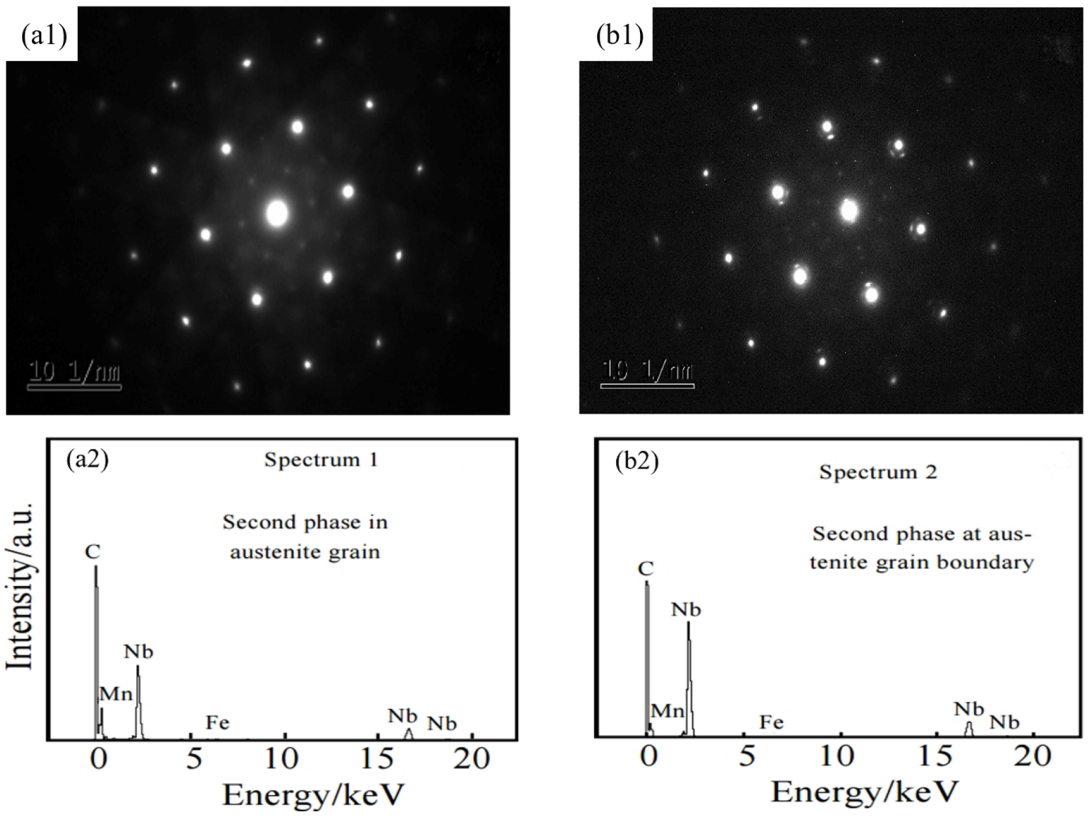


Figure 3. TEM bright field images (**a**,**b**), SAED patterns (**a1**,**b1**), and EDS analysis (**a2**,**b2**) second phase in the grain of (**a**) and at the grain boundary of (**b**) Fe-28Mn-10Al-C-0.5Nb steel Reprinted from Ref. [30].

3.2. Calculation of Mis-Energy in the Test Steel Layer

Studies have shown that for high-manganese Fe-Mn-Al-C low-density steels, variations in stacking fault energy (SFE) determine the plastic deformation mechanism of the steel, which in turn influences its mechanical properties [31]. When the SFE is less than 18 mJ/m^2, the primary strengthening mechanism in the alloy is the TRIP effect; when the SFE ranges from 18 to 45 mJ/m^2, the TWIP effect is dominant; and when the SFE exceeds 45 mJ·m^2, the strengthening mechanism is primarily dislocation slip. Therefore, calculating the stacking fault energy (SFE) is crucial for determining the deformation mechanism of the experimental steel.

Based on the thermodynamic model developed by Olson–Cohen [32,33], the calculation of SFE (τ) can be expressed as follows:

$$\tau = 2\rho\Delta G^{\gamma\to\varepsilon} + 2\sigma \quad (2)$$

$$\rho = (\frac{4}{3})(\frac{1}{\alpha^2 N}) \quad (3)$$

In the equation:

$\Delta G^{\gamma\to\varepsilon}$—Gibbs free energy required for the transition from γ_{fcc} to ε_{hcp}, kJ/mol;
P—{1 1 1} surface atomic packing density, mol/cm^3;
σ—γ/ε interface energy, J/mol;
α—γ_{fcc} lattice constant;
N—Avogadro's constant.

For a single-phase (φ) binary solution consisting of elements i and j, the Gibbs free energy G^{φ} can be expressed as follows:

$$G^{\varphi} = X_i G_i^{\varphi} + X_j G_j^{\varphi} + RT\left(X_i \ln X_i + X_j \ln X_j\right) + X_i X_j \Omega_{ij}^{\varphi} \quad (4)$$

$$\Omega_{ij}^{\varphi} = L_0^{\varphi} + L_1^{\varphi}\left(X_i - X_j\right) \quad (5)$$

$$G_{mg}^{\varphi} = f\left(\frac{T}{T_{neel}}\right) RT \ln(\beta + 1) \quad (6)$$

X—mole fraction of each phase, %;
G_{mg}^{φ}—Gibbs free energy in the magnetic state of phase φ, kJ/mol;
Ω_{ij}^{φ}—interaction parameter between the i and j phases;
L_0—temperature-based parameter;
L_1—constant;
T_{neel}—Neel temperature, K;
β—magnetic distance, value dependent on composition.

Based on Equations (4)–(6), $\Delta G^{\gamma \to \varepsilon}$ for binary austenitic steel can be approximated as follows:

$$\Delta G^{\gamma \to \varepsilon} = X_i \Delta G_i^{\gamma \to \epsilon} + X_j \Delta G_j^{\gamma \to \varepsilon} + X_i X_j \Omega_{ij}^{\gamma \to \varepsilon} + \Delta G_{mg}^{\gamma \to \epsilon} \quad (7)$$

In Fe-Mn-Al-C-Nb low-density steels, the interaction parameters of elements other than Fe, Mn, and Nb as well as the values of $\Delta G_{mg}^{\gamma \to \epsilon}$ have a small effect on the numerical changes of the layer dislocation energies, which are neglected here. Based on Equation (7) and the regular solid solution model, the "Δ" $\Delta G^{\gamma \to \varepsilon}$ of Fe-Mn-Al-C-Nb multicomponent low-density steel can be approximated as follows:

$$\begin{gathered} \Delta G^{\gamma \to \varepsilon} = X_{Fe} \Delta G_{Fe}^{\gamma \to \epsilon} + X_{Mn} \Delta G_{Mn}^{\gamma \to \varepsilon} + X_{Al} \Delta G_{Al}^{\gamma \to \epsilon} + X_C \Delta G_C^{\gamma \to \epsilon} \\ + X_{Nb} \Delta G_{Nb}^{\gamma \to \epsilon} + X_{Fe} X_{Mn} \Omega_{FeMn}^{\gamma \to \varepsilon} + X_{Fe} X_{Al} \Omega_{FeAl}^{\gamma \to \varepsilon} + X_{Fe} X_C \Omega_{FeC}^{\gamma \to \varepsilon} \\ + X_{Fe} X_{Nb} \Omega_{FeNb}^{\gamma \to \varepsilon} + X_{Mn} X_C \Omega_{MnC}^{\gamma \to \varepsilon} + \Delta G_{mg}^{\gamma \to \epsilon} \end{gathered} \quad (8)$$

Based on Equations (2) and (7) and the parameters provided in Table 3, at 20 °C room temperature, the $\Delta G^{\gamma \to \varepsilon}$ and SFE for 0Nb steel are 1083 J/mol and 81.69 mJ/m^2, respectively, and for 0.5Nb steel, they are 1128 J/mol and 84.31 mJ/m^2, respectively. These results are in close agreement with the calculations by Wu [34], indicating that both experimental steels possess stacking fault energies significantly higher than those required for the TWIP effect, suggesting that the deformation mechanism in these low-density steels is primarily dislocation slip.

Table 3. Values used for estimating the stacking fault energy (SFE) of Fe–28Mn–10Al–C–xNb steel, calculated using Equations (2), (5), and (8) [32].

Parameters	Values and Functions
ρ	2.94×10^{-5} (mol/m^2)
σ	9 (mJ/mol)
$\Delta G_{Fe}^{\gamma \to \epsilon}$	−2243.38 + 4.309T (J/mol)
$\Delta G_{Mn}^{\gamma \to \varepsilon}$	−1000 + 1.123T (J/mol)
$\Delta G_{Al}^{\gamma \to \epsilon}$	2800 + 5T (J/mol)
$\Delta G_{C}^{\gamma \to \epsilon}$	−22,166 (J/mol)
$\Delta G_{Nb}^{\gamma \to \epsilon}$	4046 (J/mol)

Table 3. *Cont.*

Parameters	Values and Functions
$\Omega_{FeMn}^{\gamma\to\varepsilon}$	$2180 + 532\ (X_{Fe} - X_{Mn})$ (J/mol)
$\Omega_{FeAl}^{\gamma\to\varepsilon}$	3339 (J/mol)
$\Omega_{FeC}^{\gamma\to\varepsilon}$	42,500 (J/mol)
$\Omega_{MnC}^{\gamma\to\varepsilon}$	26,910 (J/mol)
$\Omega_{FeNb}^{\gamma\to\varepsilon}$	27,403 (J/mol)
β^{γ}	$0.7X_{Fe} + 0.62X_{Mn} - 0.64X_{Fe}X_{Mn} - 4X_{C}$
β^{ε}	$0.62X_{Mn} - 4X_{c}$
T_{nell}^{γ}	$580X_{Mn}$ (K)
T_{nell}^{ε}	$250\ln X_{Mn} - 4750X_{Mn}X_{C} - 6.2X_{Al} + 720$ (K)
$f\left(\frac{T}{T_{neel}}\right)$	$1 - \frac{\left\{\left(\frac{79\tau^{-1}}{140\rho}\right)+\left(\frac{474}{497}\right)\left(\frac{1}{\rho}-1\right)\left(\frac{\rho^{3}}{6}\right)+\left(\frac{\tau^{6}}{135}\right)+\left(\frac{\tau^{15}}{600}\right)\right\}}{D}$ When $\tau = \frac{T}{T_{Nell}} < 1$. Where $\rho = 0.28,\ D = 2.34$ $1 - \frac{\left\{\left(\frac{\tau^{-5}}{10}\right)+\left(\frac{\tau^{-15}}{315}\right)+\left(\frac{\tau^{-25}}{1500}\right)\right\}}{D}$ When $\tau = \frac{T}{T_{Nell}} > 1$. Where $\rho = 0.28,\ D = 2.34$

3.3. Effect of Nb Alloying and Solution Treatment on the Microstructure of Cold-Rolled Test Steels

The microstructures of 0Nb and 0.5Nb low-density steels processed through cold rolling and solution treatment at 1050 °C for 30 min are presented in Figure 4. After undergoing 66% cold compression deformation, the grains in the test steels are significantly elongated and flattened along the rolling direction, leading to a noticeable lath-like morphology. Inside the elongated grains, a fibrous structure is formed, and grain size heterogeneity increases due to the lack of recrystallization at ambient temperatures. In comparison with the cold-rolled state, the high-temperature solution treatment at 1050 °C results in a microstructure composed exclusively of single-phase polygonal austenite. The boundaries of the austenite grains become well-defined, with a uniform grain size distribution and the presence of multiple twins within the grains. As illustrated in Figure 4, the austenite grains are smaller in the 0.5Nb solution-treated state, indicating that Nb alloying significantly refines the austenite grain structure. This can be attributed to the high-temperature solution treatment process, which not only removes defects introduced during cold rolling but also lowers the overall system energy. Additionally, this process leads to a partial restoration of the microstructure to its pre-deformation state through dislocation annihilation and rearrangement. The stored energy, coupled with the elevated temperature, facilitates the formation and migration of large-angle grain boundaries, thereby promoting the development of new grains and initiating recrystallization. Furthermore, thermodynamic calculations suggest that the addition of Nb promotes the formation of a secondary phase in the low-density steels. The precipitate phase exerts a pinning effect on the grain boundaries, impeding their movement and slowing down the recrystallization and growth of the grain boundaries [35]. This, in turn, effectively refines the grains and enhances mechanical properties through both grain boundary strengthening and precipitation strengthening [36,37]. The drag effect of Nb further retards the migration of grain boundaries.

As shown in Figure 4, the amount of twins in 0.5Nb steel is significantly lower than that in 0Nb steel. This phenomenon is related to the stacking fault energy of austenite in the steel. As calculated earlier, the stacking fault energy of austenite in 0.5Nb steel (84.31 mJ/m^2) is higher than that in 0Nb steel (81.69 mJ/m^2). On the one hand, twins, as a characteristic feature of overheated structures, are more likely to form in austenite crystals with lower stacking fault energy, which meets the energy requirements for their

formation [38]. On the other hand, the higher stacking fault energy in 0.5Nb steel increases the nucleation resistance of partial dislocations at grain boundaries. As a result, partial dislocations are more likely to aggregate into full dislocations, thereby suppressing the formation of twins and inhibiting the generation of twinned crystals.

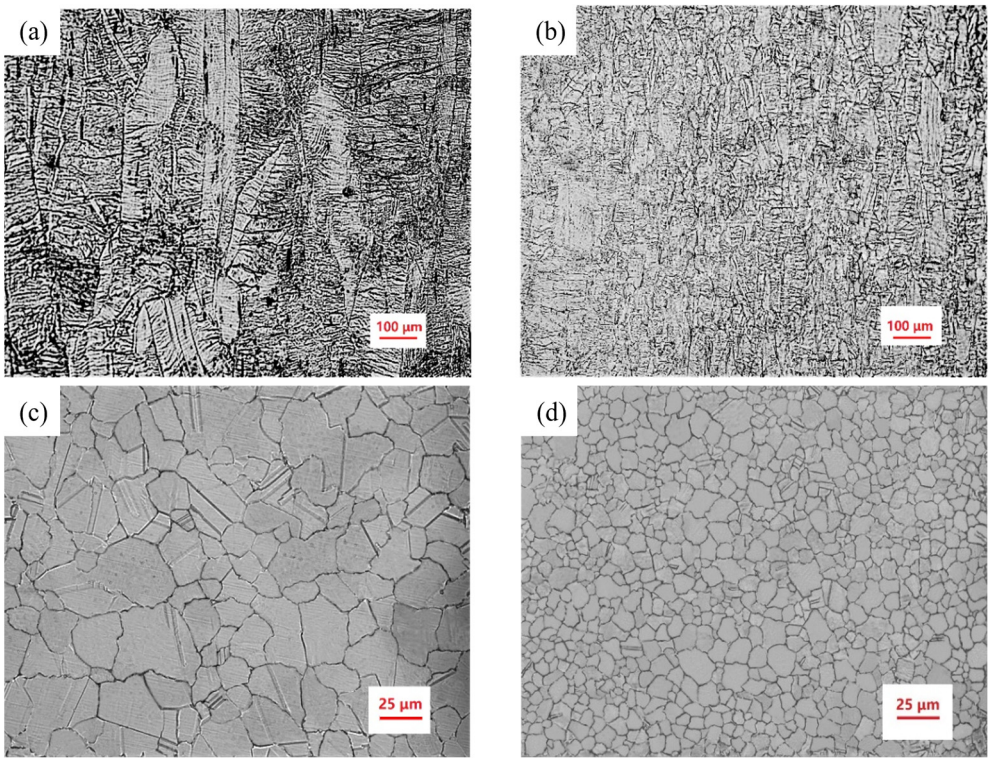


Figure 4. Microstructure of the test steels with different Nb contents after cold rolling and solution treatment: (**a**) 0Nb after cold rolling, (**b**) 0.5Nb after cold rolling, (**c**) 0Nb after solution treatment, (**d**) 0.5Nb after solution treatment.

3.4. Effect of Nb Alloying and Solution Treatment on the Mechanical Properties and Fracture Mechanism of Cold-Rolled Test Steels

(1) Influence of Nb Alloying and Solution Treatment on the Mechanical Properties

The engineering stress–strain curves of the two test steels after undergoing cold rolling and solution treatment at 1050 °C for 30 min are shown in Figure 5, with the corresponding performance parameters provided in Table 4. A comparison of the mechanical properties is depicted in Figure 6. As illustrated in Figure 5 and Table 4, following the cold rolling process, both 0Nb and 0.5Nb test steels exhibit elevated yield strength and ultimate tensile strength, both exceeding 1200 MPa. However, this deformation process leads to a considerable reduction in material ductility, with elongation at fracture ranging from 3.03% to 5.13%, which is insufficient for meeting the requirements of automotive steel applications. After solution treatment, the engineering stress–strain curves of both test steels, containing different Nb concentrations, show similar trends. Specifically, under continuous loading, both materials experience elastic deformation within a narrow strain range, quickly reaching the specified plastic elongation strength before transitioning to plastic deformation. During this stage, external stress increases in proportion to the strain, indicating continuous strain hardening behavior. Compared to the cold-rolled state, after the high-temperature solution treatment, the elongation at fracture of the two steels increases substantially, ranging from 38.14% to 44.45%, with the Nb-containing low-density steel exhibiting superior ductility. This improvement can be attributed to the microstructural changes induced by the solution treatment. The cold rolling process disrupts the

microstructure, resulting in elongated grains and a fibrous texture, which leads to high strength but poor toughness. Microstructural observations show that the high-temperature solution treatment eliminates cold deformation-induced defects, promoting the formation of austenite grains with uniform size distribution through recrystallization. This effectively prevents stress concentration during room-temperature stretching, enhances coordinated deformation between grains, and eliminates work hardening. Consequently, post-fracture elongation increases significantly, from a maximum of 5.13% to 38.14% to 44.45%. Moreover, the addition of Nb elements further refines the austenite grains, increasing the density of grain boundaries per unit area. This results in deformation being distributed across a greater number of grains during the stretching process, reducing dislocation pile-up within individual austenite grains. This helps achieve more uniform deformation, minimizes the likelihood of stress concentration, and improves the material's ductility.

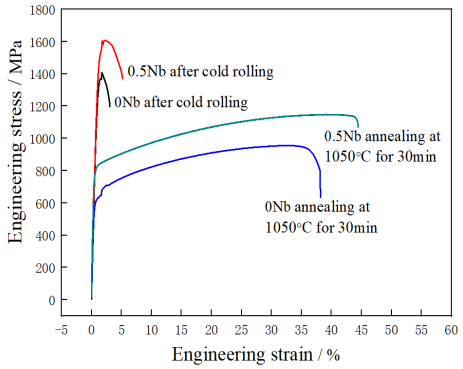


Figure 5. Engineering stress–strain curves of low-density steels subjected to cold rolling and solution treatment at 1050 °C for 30 min with different Nb contents.

Table 4. Mechanical properties of 0Nb and 0.5Nb low-density steels after cold rolling and solution treatment.

Steel	State	YS/MPa	UTS/MPa	El/%	PSE/MPa·%
0Nb	Cold rolling	1279	1407	3.03	4.26
0Nb	Solution treatment	591	955	38.14	36.42
0.5Nb	Cold rolling	1409	1605	5.13	8.23
0.5Nb	Solution treatment	795	1146	44.45	50.94

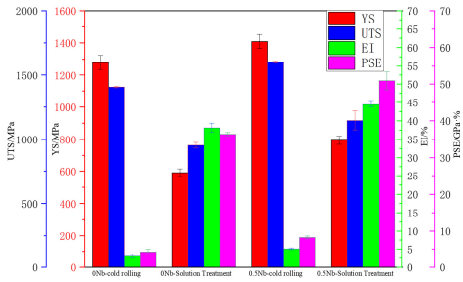


Figure 6. Comparison of the mechanical properties of 0Nb and 0.5Nb low-density steel after cold rolling and solution treatment.

The high-temperature solution treatment applied to the low-density steels not only improves their ductility but also enhances their yield strength (YS) and ultimate tensile strength (UTS). For instance, the 0.5Nb steel shows significant increases in these properties, reaching 795 MPa for YS and 1146 MPa for UTS, which represents substantial gains over the 0Nb steel. Table 5 presents the mechanical property indexes of Fe-Mn-Al-C steels with different compositions subjected to various treatments [39]; PSE stands for strong

plastic accumulation of materials (product of strength and elongation), and EI is the elongation at break. It can be observed that the strong plasticity level of 0.5Nb steel within the given composition range is among the highest in its category of low-density steels. Notably, its strength surpasses 1000 MPa, and its elongation at break exceeds 50%, which reflects significant property improvements. The observed changes are attributed to the deformation and strengthening mechanisms in Fe-Mn-Al-C-Nb low-density steel. Based on previous layer dislocation energy calculations, the dislocation energy in both test steels is considerably higher than the threshold required for the TWIP effect. Therefore, the deformation of these steels is governed by dislocation slip. The addition of Nb not only refines the austenite grains within the material but also increases the number of grain boundaries in a given volume, which in turn impedes dislocation movement. The higher energy at these boundaries restricts dislocation planar slip, thereby limiting the material's plastic deformation and enhancing the overall strength of the steel matrix. Thermodynamic calculations using Thermo-Calc further reveal that the presence of Nb promotes the formation of a precipitate phase within the steel, which obstructs dislocation movement during tensile testing. This precipitate phase impedes the slip of dislocations, providing a strengthening effect that increases both yield and ultimate tensile strength. As a result, the steel retains high strength after solution treatment, with the 0.5Nb steel showing superior mechanical properties compared to the 0Nb steel. Additionally, the solution treatment enhances both strength and ductility, significantly improving the strong plasticity index. As shown in Table 4, after treatment at 1050 °C, both test steels exhibit an optimal balance of ductility and strength. The 0.5Nb low-density steel, in particular, demonstrates an exceptionally high product of strength and elongation (PSE) value of 50.94 GPa-%, surpassing traditional automotive TRIP and TWIP steels. This confirms that Nb-alloyed low-density steels achieve an excellent balance between strength and toughness after cold rolling and solution treatment.

Table 5. Comparison of the room temperature mechanical properties of Fe-Mn-Al-C steels with different compositions and processes.

Composition (wt.%)	TE (%)	UTS (MPa)	PSE/MPa·%	Thermal/Mechanical Processes
Fe-28Mn-10Al-C-0.5Nb	44.45	1146	50.94	Cold rolling/solution
Fe-23Mn-1.5Al-0.3C [40]	98.9	840	83.08	Hot rolling/solution
Fe-25Mn-10Al-1.1C [41]	62	913	56.6	Solution/water quenching
Fe-11Mn-10Al-1.2C [42]	35.4	1183	41.88	Solution/water quenching
Fe-30Mn-11Al-1.2C [43]	17.8	1218	21.68	Solution/aging
Fe-21Mn-10Al-C-5Ni [44]	80	775	62.00	Solution/water quenching
Fe-29Mn-9.4Al-0.3C [45]	30	757	22.71	Cold rolling/annealing
Fe-13.6Mn-1.2Al-0.6C [46]	74	1120	82	Solution/water quenching

(2) Tensile Fracture Morphology of Solution-Treated, Low-Density Steel: Effect of Nb Alloying

As shown in Figure 7, the SEM images depict the tensile fracture morphology of the two test steels in the cold-rolled condition after solution treatment at 1050 °C for 30 min. As observed in Figure 7, the tensile fracture of the test steels, both before and after Nb alloying, consists of equiaxed ligament nests of uniform size, as indicated by the arrows in the figure. Notably, the fracture morphology does not display the characteristic "icing sugar" block structure or shear bands across the grains, indicating that the fracture mechanism of the test steels is ductile fracture after solution treatment. Furthermore, the size and depth of the toughness nests are influenced by the steel's composition. Specifically, the Nb-free Fe-28Mn-10Al-C low-density steel exhibits smaller and shallower toughness nests. The refining of the austenite grain size in the steel through Nb alloying enhances

the fine-grain strengthening mechanism. Consequently, the fracture strain of 0.5Nb steel (44.41%) is higher than that of 0Nb steel (38.14%). The addition of Nb also delays plastic destabilization, resulting in a longer crack propagation cycle for 0.5Nb steel. As a result, the proportion of elongated ligamentous nests in the steel increases significantly, accompanied by a gradual enlargement of the ligamentous nests, while the number of such nests per unit area decreases markedly.

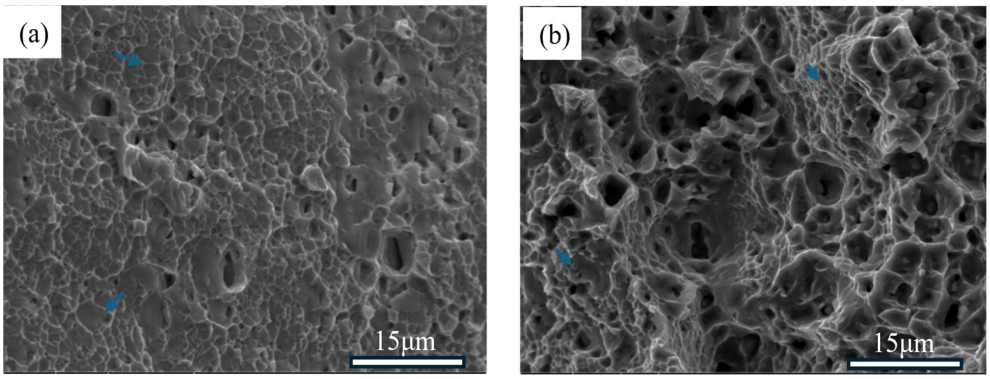


Figure 7. Fractography of specimens with different Nb contents after solution treatment at 1050 °C for 30 min: (**a**) 0Nb, (**b**) 0.5Nb.

3.5. Effect of Solution Treatment Temperature on the Microstructure and Mechanical Properties of 0.5Nb-Containing Test Steel

(1) Influence of Solution Treatment Temperature on the Microstructure of 0.5Nb-Containing Test Steel

The phase composition of the aged steel treated at solution treatment temperatures ranging from 950 to 1050 °C for 30 min was examined using XRD analysis. The XRD results are shown in Figure 8. At solution treatment temperatures of 950 and 1000 °C, the experimental steel predominantly consists of the austenite phase, with a small amount of ferrite phase. Notably, at 950 °C, a distinct κ-carbide diffraction peak appears to the left of the austenite (111) diffraction peak. At 1050 °C, the steel is predominantly austenitic. Due to the limitations of XRD detection, some precipitate phases with low content may not have been detected.

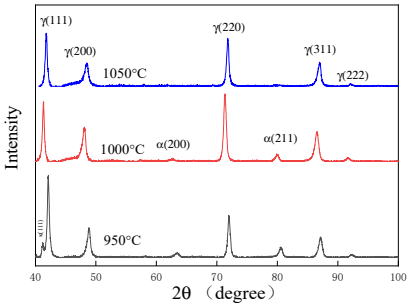


Figure 8. XRD diffraction patterns of 0.5Nb low-density steel after different solution treatment temperature treatments.

Figure 9 illustrates the metallographic microstructure of 0.5Nb steel in the cold-rolled state after solution treatment at 950 °C, 1000 °C, and 1050 °C. It can be observed that the high concentration of austenitic elements, such as Mn and C, in the steel results in a microstructure composed of single-phase austenite. The boundaries of the polygonal austenite grains are clearly delineated, and twins are visible within certain grains. As the solution treatment temperature rises from 950 °C to 1050 °C, the austenite grain sizes gradually increase, resulting in a decreased grain boundary density. This can be attributed

to the increased diffusion of alloying elements, such as C and Mn, with rising solution treatment temperature, which enhances the migration rate of austenite grain boundaries. As a result, higher solution treatment temperatures accelerate the growth of austenite grains in 0.5Nb steel within the same heat treatment period. Figure 9 also reveals that at a solution treatment temperature of 950 °C, the lower temperature results in an insufficient driving force for twin growth, and the migration rate of twin boundaries is relatively slow, preventing the formation of distinct twins. As the solution treatment temperature rises, the twin crystals progressively grow along the direction perpendicular to the austenite grain boundaries, eventually forming twins that span across multiple austenite grains. With further increases in the solution treatment temperature, the migration rate of twin boundaries accelerates, leading to a gradual increase in the number of twins.

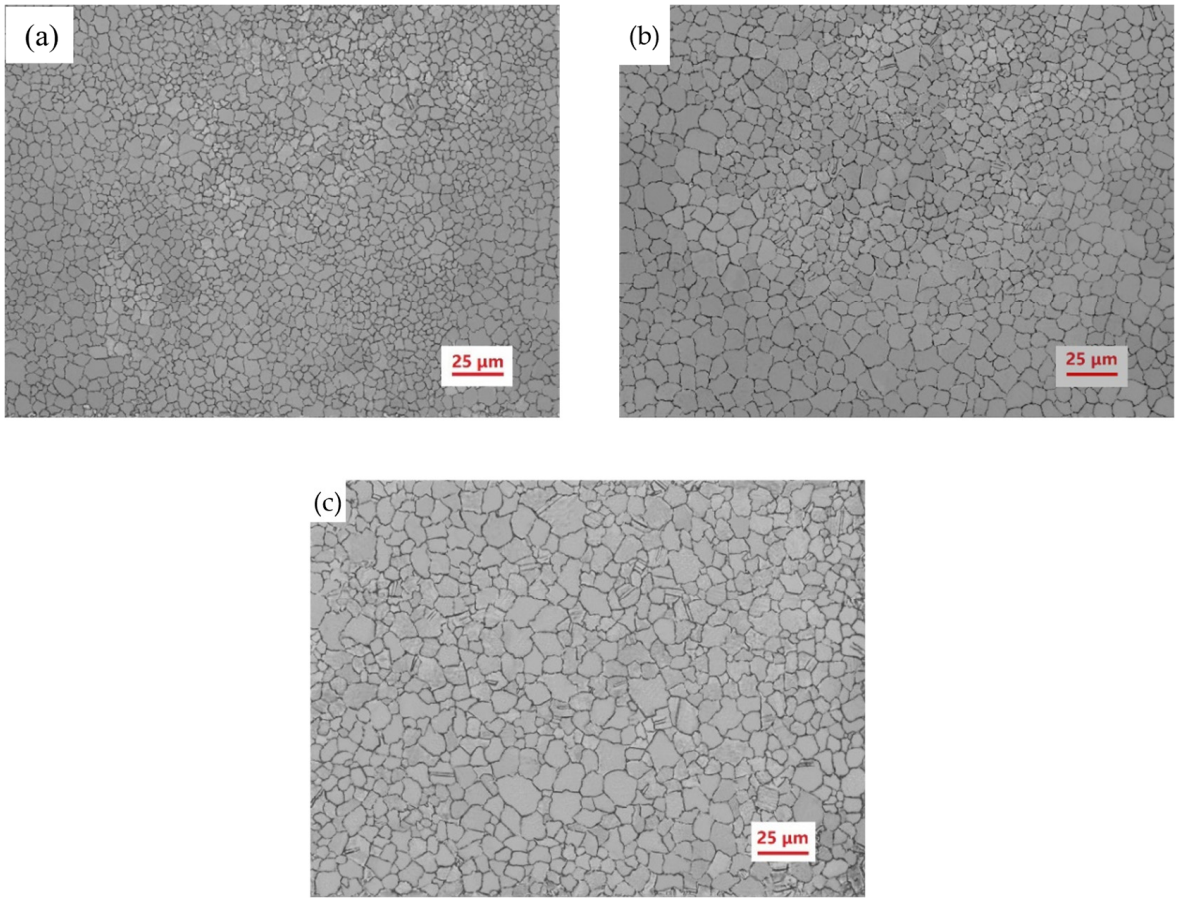


Figure 9. Microstructure of 0.5Nb low-density steel at different solution treatment temperatures: (**a**) 950 °C, (**b**) 1000 °C, (**c**) 1050 °C.

(2) Mechanical Properties and Work-Hardening Behaviors of 0.5Nb Test Steels at Various Solution Treatment Temperatures

The engineering stress–strain curves of 0.5Nb steel after a 30 min solution treatment at 950 °C, 1000 °C, and 1050 °C are presented in Figure 10. Figure 11 shows a comparison of the mechanical properties, with the corresponding mechanical property values and calculations of the product of strength and elongation (PSE) shown in Table 6. It is evident that the deformation process of 0.5Nb steel after cold rolling and high-temperature solution treatment at different temperatures is characterized by plastic deformation. As the solution treatment temperature increases, the strength of the 0.5Nb steel gradually decreases, while the post-fracture elongation increases substantially. When the solution treatment temperature exceeds 1000 °C, the low-density steel demonstrates an ultimate

tensile strength greater than 1100 MPa, along with an elongation at break exceeding 40% and a PSE surpassing 50 GPa-%. Consequently, the role of solution treatment in optimizing the mechanical properties becomes more pronounced.

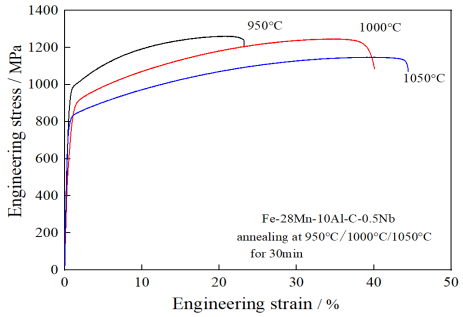


Figure 10. Engineering stress–strain curves of Fe-28Mn-10Al-C-0.5Nb low-density steel subjected to different solution treatment temperatures.

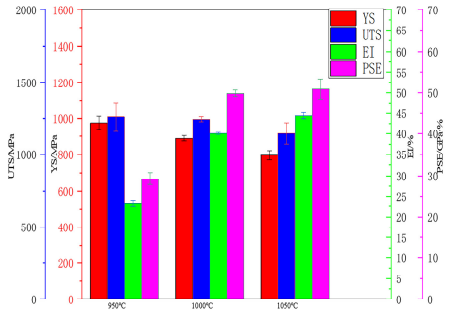


Figure 11. Comparison of mechanical properties of Fe-28Mn-10Al-C-0.5Nb low-density steel at different solution treatment temperatures.

Table 6. Mechanical properties of 0.5Nb steel after solution treatment at different temperatures for 30 min.

Steel	YS/MPa	UTS/MPa	El/%	PSE/MPa·%
950 °C	975	1260	23.25	29.3
1000 °C	889	1244	40.07	49.85
1050 °C	795	1146	44.45	50.94

This phenomenon can primarily be attributed to the fact that, with increasing solution treatment temperature, the austenite grains in low-density steel grow, significantly enhancing the range of dislocation slip during tensile deformation. This reduces the stress concentration caused by dislocation accumulation and improves the uniformity and coordination of the material's deformation, ultimately resulting in enhanced ductility at higher solution treatment temperatures. Concurrently, the elevated solution treatment temperature causes austenite grain coarsening, which reduces the grain boundary density. As a result, the hindering effect of grain boundaries on dislocation slip during tensile deformation is diminished, leading to a reduction in both the yield strength and ultimate tensile strength of the material during the solution treatment process. Specifically, when the austenite grains in the test steel grow too large, the fine grain strengthening effect is weakened, leading to a greater loss in the material's strength and, consequently, a decline in overall performance. For instance, as shown in Table 6, the 0.5Nb test steel, after solution treatment at 1000 °C for 30 min, achieved the optimum overall performance, with the product of strength and elongation (PSE) as high as 49.85 GPa-%. However, as the solution treatment temperature increases to 1050 °C, both the yield strength and ultimate tensile

strength decrease significantly, while the increase in elongation after fracture is marginal. This results in the comprehensive mechanical properties being slightly inferior to those obtained at the 1000 °C solution treatment state. Therefore, under the experimental conditions of the steel composition, the optimal overall performance can be achieved through high-temperature solution treatment at 1000 °C.

Figure 12 illustrates the fracture micro-morphology of 0.5Nb steel at three different solution treatment temperatures. As shown in Figure 12, the fracture morphology of the test steels after solution treatment at different temperatures consists predominantly of numerous tough nests, as indicated by the arrows in the figure. This is attributed to the fact that in Fe-28Mn-10Al-C-0.5Nb low-density steels, which possess higher dislocation energies, the material's fracture failure process is typically initiated by dislocation slip, with the formation of micropores during plastic deformation. In the plastic deformation stage, as the strain increases, the microcracks caused by dislocation slip will expand along, causing the holes to gather to form tough nests. When the strain increases to a certain degree, the tough nests connect with each other to form micropores, leading to ductile fracture failure of the material. Therefore, the formation and aggregation of micropores represent the primary fracture mechanism of the highly ductile 0.5Nb low-density steel at various solution treatment temperatures. Additionally, with increasing solution treatment temperature, the austenite grain size in 0.5Nb low-density steel increases, which enhances the coordination and homogeneity of deformation. As a result, dislocations have a longer free range along the slip surface during the tensile process, allowing for more extensive microcrack propagation and void aggregation. Consequently, as shown in Figure 11, high-temperature solution treatment specimens exhibit larger and deeper ligamentous nests at the fracture.

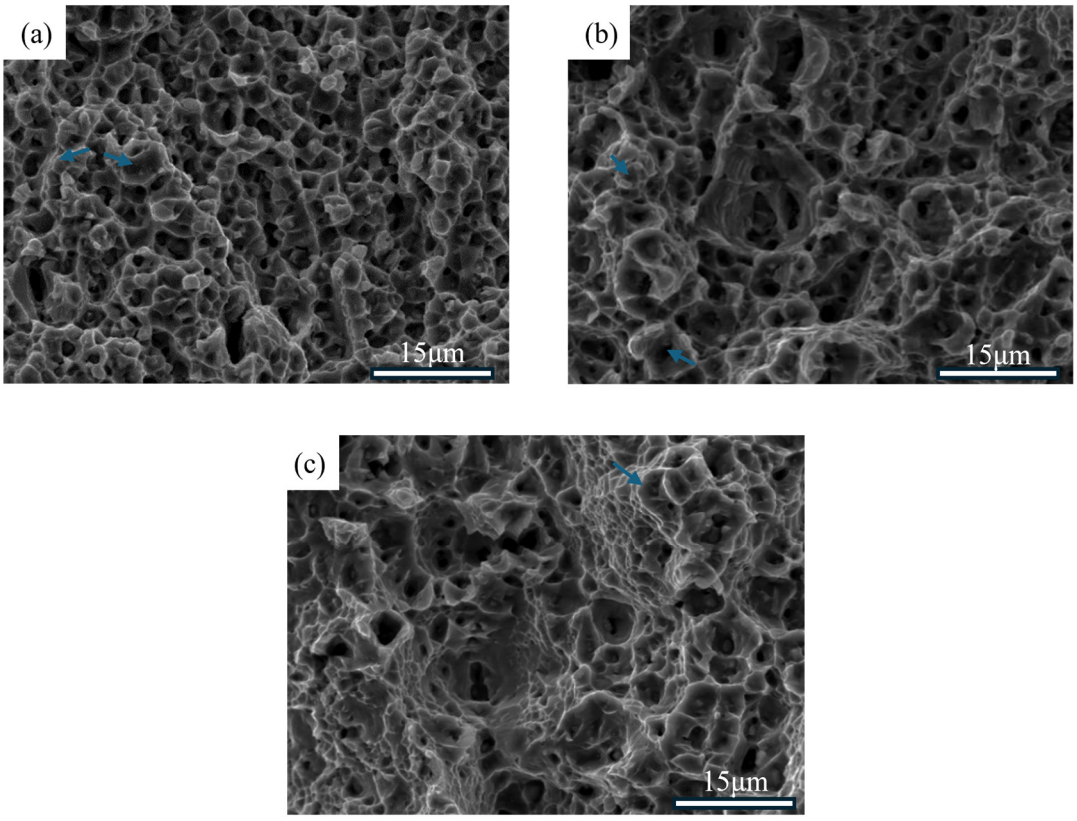


Figure 12. Fractograph of Fe-28Mn-10Al-C-0.5Nb low-density steel after solution treatment at different temperatures: (**a**) 950 °C, (**b**) 1000 °C, (**c**) 1050 °C.

The work hardening ($d\sigma/d\varepsilon$) curves of 0.5Nb steel subjected to solution treatment at temperatures ranging from 950 °C to 1050 °C for 30 min are presented in Figure 13. Initially, at true strains below 0.09, the steel treated at 950 °C exhibited a significantly higher rate of work hardening. However, as the solution treatment temperature increases, for the same level of strain, a decrease in work hardening rate is observed in the lower strain range. In contrast, when the true strain increases further, the steel solution treated above 1000 °C maintains a consistently high work hardening rate during deformation. Moreover, higher solution treatment temperatures correlate with a greater true strain required before a noticeable drop in work hardening rate occurs. In other words, the material experiences failure or fracture only at higher true strains when subjected to higher solution treatment temperatures, suggesting that these temperatures effectively delay the onset of plastic destabilization, enhancing the ductility of the steel. This behavior can be explained by the high dislocation energy in Fe-28Mn-10Al-C-0.5Nb steel, where the primary plastic deformation mechanism is dislocation slip induced by external stresses. The strengthening of the material is achieved by impeding the slip of dislocations during deformation. Tensile tests performed by other researchers within our team on steels with similar compositions but varying deformation levels, as shown in Figure 14 [33], further support these observations. In Figure 14a, at a tensile strain of 0.05, bright-field transmission electron microscopy (TEM) images reveal a typical planar slip structure along {111} planes within individual slip systems, indicating the development of substructures. With increasing external stress and deformation, the dislocation structure remains in planar slip form without forming dislocation cells. Additionally, another planar slip trajectory, identified as a Taylor lattice, emerges in the deformed microstructure, as seen in Figure 14b. In Figure 14c, a bright-field TEM image at a deformation level of 0.25 shows clear microbands (labeled as A in the figure), which are characteristic of low-density steel. The continuous multiplication and slip of dislocations lead to the accumulation of a large number of dislocations, which further reduces the spacing between the slip bands. The deformation process leads to the formation of well-defined microband structures, particularly at the grain boundaries of the deformed sample, as indicated by the label "B" in Figure 14c. The bright-field TEM image in Figure 14d reveals the fractured surface of the steel, where finer, more robust microband structures are observed. These structures not only appear as distinct bands but also exhibit intersecting microbands. The study highlights the influence of Nb alloying and the precipitation of precipitate phases on the strengthening of 0.5Nb steel. These mechanisms include solid solution strengthening, grain refinement, and precipitation strengthening, all of which hinder dislocation movement and contribute to the enhancement of the material's strength. Given the stable thermodynamic properties of Nb precipitate phases [47,48], solution treatment temperature plays a crucial role in influencing the strain-hardening behavior of the steels by altering the size of austenite grains and modifying lattice friction. At lower solution treatment temperatures, the finer austenite grains increase the density of grain boundaries, which significantly restricts dislocation slip during deformation. Consequently, the strength of the steel increases quickly, and the work-hardening rate remains high. However, at lower temperatures, the small grain size restricts the movement of dislocations during plastic deformation, which leads to the saturation of dislocation density and the termination of dislocation slip at lower strains. Once saturation is reached, the work-hardening rate decreases sharply, eventually becoming negative and leading to fracture. As the solution treatment temperature increases, the austenite grain size expands, reducing the obstruction to dislocation slip at the grain boundaries. During the early stages of plastic deformation, the material exhibits a lower work-hardening rate. As deformation continues, however, more dislocations form, resulting in an increase in dislocation density. This triggers the activation of additional slip systems, producing new dislocations that strengthen the matrix,

allowing the 0.5Nb steel to maintain a consistently high work-hardening rate throughout the deformation process. Consequently, with the rise in solution treatment temperature, the strain hardening rate decreases under the same strain, while the true strain required for fracture failure increases. These observations suggest that higher solution treatment temperatures effectively delay plastic destabilization during tensile deformation, thereby improving the material's plasticity.

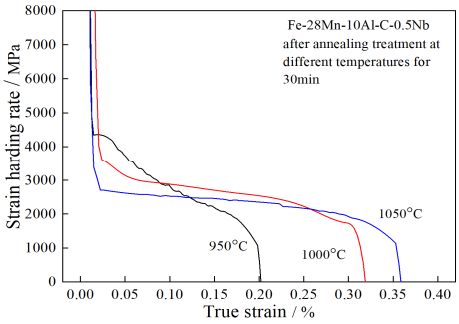


Figure 13. True strain hardening rate curve of Fe-28Mn-10Al-C-0.5Nb low-density steel after solution treatment at different temperatures for 30 min.

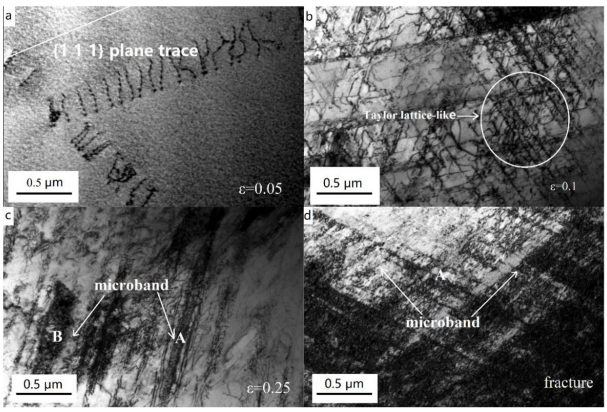


Figure 14. TEM micrographs of the Fe–28Mn–10Al–C–0.5Nb low-density steel after interrupted at different strains during room temperature tensile deformation of (**a**) 5%, (**b**) 10%, (**c**) 25%, and (**d**) failure to fracture, reprinted from [33].

4. Conclusions

Thermodynamic simulations performed using Thermo-Calc reveal that the addition of Nb when the system is at equilibrium significantly hinders the decomposition of austenite and encourages the formation of precipitate phases in Fe-28Mn-10Al-C low-density steels. Furthermore, Nb is almost entirely incorporated as precipitates of a second phase. The high-temperature solution treatment effectively eliminates the defects caused by cold rolling, leading to the development of uniform single-phase polygonal austenite grains. In contrast to the cold-rolled condition, the elongation of both test steels after solution treatment increases substantially, rising from a maximum of 5.13% to 38.14% and 44.45%, respectively. This treatment optimizes the balance between strength and toughness while also enhancing both yield strength and ultimate tensile strength. The mechanical properties of the Nb-containing steels are superior to those of the 0Nb test steels. As the solution treatment temperature increases, the austenite grain size in the 0.5Nb low-density steel grows, and the number of twins increases. While the yield strength and ultimate tensile strength gradually decrease, a significant improvement in toughness is observed.

Author Contributions: Conceptualization, L.H. and T.M.; methodology, Y.L. and T.M.; software, L.H. and J.G.; validation, X.W., J.G. and T.M.; formal analysis, L.H. and P.X.; investigation, J.G., P.X. and X.W.; resources, L.H.; data curation, Y.L. and T.M.; writing—original draft preparation, L.H. and T.M.; writing—review and editing, T.M.; visualization, L.H.; supervision, T.M.; project administration, T.M. and Y.L.; funding acquisition, Y.L. All authors have read and agreed to the published version of the manuscript.

Funding: This study was supported by the Tangshan Science and Technology Program (No. 22130223H), the National Natural Science Foundation of China (No. 51974129), and the Hebei Province Graduate Student Innovation Program (No. CXZZSS2024052).

Data Availability Statement: The original contributions presented in the study are included in the article, further inquiries can be directed to the corresponding author.

Conflicts of Interest: The authors declare no conflicts of interest.

References

1. Ding, H.; Liu, D.; Cai, M.; Zhang, Y. Austenite-Based Fe-Mn-Al-C Lightweight Steels: Research and Prospective. *Metals* **2022**, *12*, 1572. [CrossRef]
2. Wu, Z.; Liu, S.; Hasan, M.; Li, E.; An, X. The hot deformation behavior in austenite-ferrite heterostructured low density Fe-Mn-Al-C steel. *Mater. Today Commun.* **2023**, *37*, 107184. [CrossRef]
3. Ren, J.; Zhang, L.; Li, Z.; Chen, J.; Zhang, W.; Wu, S.; Liu, Z. Fe-Mn-Al-C high-entropy steels with superior mechanical properties at 4.2 K. *Mater. Des.* **2023**, *228*, 111840. [CrossRef]
4. Kang, J.; Li, Y.; Wang, X.; Wang, H.; Yuan, G.; Misra, R.D.K.; Wang, G. Design of a low density Fe-Mn-Al-C steel with high strength-high ductility combination involving TRIP effect and dynamic carbon partitioning. *J. Mater. Sci. Eng. A* **2018**, *742*, 464–477. [CrossRef]
5. Chen, P.; Chen, R.; Li, X. Tensile deformation behavior related with strain-induced martensitic transformation in a duplex Fe-Mn-Al-C low-density steel. *Mater. Charact.* **2022**, *189*, 111954. [CrossRef]
6. Riaz, T.; Das, S.R.; Sahu, P. Influence of Al Variation on the Mechanical Properties and Critical Shear Stress of Twinning in Fe-Mn-Al-C Steels. *J. Mater. Eng. Perform.* **2022**, *32*, 1636–1644. [CrossRef]
7. Rodríguez, J.S.; Duran, J.F.; Aguilar, Y.; Alcazar, G.A.; Perez, T.; Zambrano, O.A. Effect of Al content on the low-stress abrasive wear behaviour of Fe-18Mn-xAl-0.7C alloys. *J. Tribol. Int.* **2023**, *180*, 108286. [CrossRef]
8. Howell, R.A.; Van Aken, D.C. A literature review of age hardening Fe-Mn-Al-C alloys. *Iron Steel Technol.* **2009**, *6*, 193–212.
9. Chen, Z.; Liu, M.; Zhang, J.; Yang, L.; Zhang, Y.; Song, C.; Zhai, Q.; Kang, J. Effect of annealing treatment on microstructures and properties of austenite-based Fe-28Mn-9Al-0.8C lightweight steel with addition of Cu. *China Foundry* **2021**, *18*, 207–216. [CrossRef]
10. Xie, Z.; Hui, W.; Bai, S.; Zhang, Y.; Zhao, X.; Li, B. Effects of annealing temperature and V addition on microstructure and mechanical properties of Fe-Mn-Al-C austenitic low-density steel. *Mater. Today Commun.* **2023**, *35*, 106328. [CrossRef]
11. Pang, J.; Zhou, Z.; Zhao, Z.; Tang, D.; Liang, J.; He, Q. Tensile Behavior and Deformation Mechanism of Fe-Mn-Al-C Low Density Steel with High Strength and High Plasticity. *Metals* **2019**, *9*, 897. [CrossRef]
12. Liu, D.; Ding, H.; Cai, M.; Han, D. Mechanical behaviors of a lower-Mn-added Fe-11Mn-10Al-1.25C lightweight steel with distinguished microstructural features. *Mater. Lett.* **2019**, *242*, 131. [CrossRef]
13. Zhou, N.; Song, R.; Yang, F.; Li, X.; Li, J. Influence of Annealing Temperature on Microstructure and Three-Stage Strain Hardening Behavior in Cold-Rolled Fe-Mn-Al-C Steel. *JOM* **2019**, *71*, 4105–4113.
14. Zheng, C.; Liu, Q.; Zheng, S.; Chong, X.; Jiang, Y.; Feng, J. Effect of solution treatment on mechanical properties and microstructure of welded joints of Fe-29Mn-9Al-0.9C low-density steel. *J. Micromechanics Mol. Phys.* **2020**, *5*, 2050006.
15. Mykhailo, V.; Anastasiia, S.; Volodymyr, S. Microstructure, mechanical and high temperature properties of cast high Mn low-density steels alloying by small Lanthanum additions. *Mater. Lett.* **2024**, *355*, 135421.
16. Ding, F.; Guo, Q.; Hu, B.; Xu, Y.; Lai, W.; Zhang, C.; Jin, X.; Luo, H. Influences of Cu alloying on precipitation, austenitic reversion and mechanical properties of NiAl-strengthened medium-Mn steels. *Acta Mater.* **2025**, *284*, 120623.
17. Sha, Q.; Sun, Z. Grain growth behavior of coarse-grained austeniteinaNb-V-Ti micro alloyed steel. *Mater. Sci. Eng. A* **2009**, *523*, 77.
18. Ma, T.; Li, H.; Gao, J.; Wang, X.; Song, H.; Li, Y. Progress on Strengthening Mechanism and Tensile Properties of Fe-Mn-Al-C Low Density Steel and Prospect of Nb Microalloying. *Mater. Rep.* **2020**, *34*, 23154–23164.
19. Zhang, D.; Liu, G.; Zhang, K.; Sun, X.; Liang, X.; Yong, Q. Effect of Nb microalloying on microstructure evolution and mechanical properties in low carbon medium manganese steel. *Mater. Sci. Eng. A* **2021**, *824*, 141813. [CrossRef]

20. Cui, D.; Chen, P.; Wang, P.; Li, X. On the Factors Influencing the High Stretch–Flangeability of a Low-Density 1180 MPa Fe–Mn–Al–C–Nb δ-QP Steel. *Acta Metall. Sin. Engl. Lett.* **2024**, *37*, 1291–1300.
21. Ramos-Fabián, N.I.; Mejía, I.; García-Domínguez, M.; Bedolla-Jacuinde, A. Metallographic, structural and mechanical characterization of a low-density austenitic Fe–Mn–Al–C steel microalloyed with Nb in hot-rolling condition. *MRS Adv.* **2023**, *8*, 1291–1295. [CrossRef]
22. Huo, W.; Song, R.; Zhang, Z.; Wang, Y.; Zhou, N.; Zhao, S.; Zhang, Y.; Sun, J. Effect of Nb contents on microstructure characteristics and yielding behavior of Fe–4Mn–2Al-0.2C steel. *Mater. Sci. Eng. A* **2021**, *819*, 141457. [CrossRef]
23. Zhao, T.; Chen, C.; Wang, Y.; Wang, T.; Sheng, G.; He, Y. Effect of NbeV microalloying on low-cycle fatigue property of Fe-Mn-Al-C austenitic steel. *J. Mater. Res. Technol.* **2023**, *23*, 3711–3725.
24. Zhuang, L.; Wang, Y.; Cheng, X.; Li, Z.; Du, J.; Li, S. The effect of Ti–Mo–Nb on the microstructures and tensile properties of a Fe–Mn–Al–C austenitic steel. *Mater. Sci. Eng. A* **2020**, *780*, 139220.
25. Lee, J.; Park, S.; Kim, H.; Park, S.J.; Lee, K.; Kim, M.Y.; Madakashira, P.P.; Han, H.N. Simulation of κ-Carbide Precipitation Kinetics in Aged Low-Density Fe–Mn–Al–C Steels and Its Effects on Strengthening. *Met. Mater. Int.* **2018**, *24*, 702–710. [CrossRef]
26. Gao, Z.; Kang, Q.; An, X.; Wang, H.; Wang, C.; Cao, W. Enhanced mechanical properties of a Fe-Mn-Al-C austenitic low-density steel by increasing hot-rolling reduction. *Mater. Charact.* **2023**, *204*, 113237. [CrossRef]
27. Park, S.W.; Park, J.Y.; Cho, K.M.; Jang, J.H.; Park, S.J.; Moon, J.; Lee, T.H.; Shin, J.H. Effect of Mn and C on age hardening of Fe-Mn-Al-C lightweight steels. *Met. Mater. Int.* **2019**, *25*, 683.
28. Liu, P.C.; Xu, X.Y.; Liu, Q.N.; Li, J.Z.; Liu, D.; Yan, Z.P.; Sun, M.Y.; Wang, X.M. Solid solution precipitation behavior of Nb in high alumina ferritic steel. *J. Eng. Sci.* **2019**, *41*, 882–888.
29. Yong, Q.L.; Zheng, L.; Sun, Z.B. Preliminary study on ordered NbC in Nb-containing microalloyed steels. *J. Met.* **1986**, *6*, 81–83.
30. Ma, T.; Gao, J.; Li, H.; Meng, X.; Li, Y. Effect of Nb on the Microstructure and Mechanical Properties of Fe-28Mn-10Al-C Low Density Steel. *Rare Met. Mater. Eng.* **2021**, *50*, 0860–0866.
31. Song, W.; Ingendahl, T.; Bleck, W. Control of strain hardening behavior in high-Mn austenitic steels. *Acta Metall. Sin.* **2014**, *27*, 546–556. [CrossRef]
32. Yoo, J.D.; Park, K.T. Microband-induced plasticity in a high Mn–Al–C light steel. *Mater. Sci. Eng. A* **2008**, *496*, 417–424. [CrossRef]
33. Ma, T.; Gao, J.; Li, H.; Li, C.; Zhang, H.; Li, Y. Microband-Induced Plasticity in a Nb Content Fe–28Mn–10Al–C Low Density Steel. *Metals* **2021**, *11*, 345. [CrossRef]
34. Wu, Z.Q. Research on Organizational Properties and Deformation Mechanism of High Strength and High Plasticity Low Density Steel. Ph.D. Thesis, Northeastern University, Shenyang, China, 2015.
35. She, Y.; Zhang, Z.; Ju, J.; Jin, B. Phase Transformation Behavior of Niobium Containing Microalloyed Steel with Predeformation and Continuous Cooling. *Mater. Sci. Forum* **2014**, *804*, 281–284. [CrossRef]
36. Wang, J.; Liu, D.; Yan, D. Austenite Growth Behavior and Prediction Modeling of Ti Microalloyed Steel. *Materials* **2024**, *17*, 3236. [CrossRef] [PubMed]
37. Liao, W.; Mazánová, V.; Heczko, M.; Hou, W.; Procario, J.; Mills, M.; Liu, X. Underlying mechanisms for the effect of Nb micro-alloying on the elemental distribution and precipitation behavior in the X70 weld metal. *Materialia* **2024**, *38*, 102264. [CrossRef]
38. Duan, F.; Lin, Y.; Pan, J.; Zhao, L.; Guo, Q.; Zhang, D.; Li, Y. Ultra-strong nano twinned pure nickel with extremely fine twin thickness. *Sci. Adv.* **2021**, *27*, 5113. [CrossRef]
39. Bai, S.; Chen, Y.; Liu, X.; Lu, H.-H.; Bai, P.-K.; Li, D.; Huang, Z.; Li, J. Research status and development prospect of Fe-Mn-C-Al system low-density steels. *J. Mater. Res. Technol.* **2023**, *25*, 1537–1559. [CrossRef]
40. Zhang, J.; Raabe, D.; Tasan, C.C. Designing duplex, ultrafine-grained Fe-Mn-Al-C steels by tuning phase transformation and recrystallization kinetics. *Acta Mater.* **2017**, *141*, 374–387. [CrossRef]
41. Xie, Z.; Hui, W.; Zhang, Y.; Zhao, X. Effect of Cu and solid solution temperature on microstructure and mechanical properties of Fe-Mn-Al-C low-density steels. *J. Mater. Res. Technol.* **2022**, *18*, 1307–1321. [CrossRef]
42. Wang, H.; Liang, Y.; Hao, S.; Wang, J.; Shi, H. Heterogeneous Fe-Mn-Al-C lightweight steel breaking the strength-ductility trade-off via high-temperature warm rolling process. *Mater. Charact.* **2024**, *218*, 114571. [CrossRef]
43. Moon, J.; Park, S.J.; Jang, J.H. Investigations of the microstructure evolution and tensile deformation behavior of austenite Fe-Mn-Al-C lightweight steels and the effect of Mo addition. *Acta Mater.* **2018**, *147*, 226. [CrossRef]
44. Ren, P.; Chen, X.; Yang, M.; Liu, S.; Cao, W. Effect of early stage of k-carbides precipitation on tensile properties and deformation mechanism in high Mn-Al-C austenitic lowdensity steel. *Mater. Sci. Eng. A* **2022**, *857*, 144132. [CrossRef]
45. Haase, C.; Barrales-Mora, L.A.; Molodov, D.A.; Gottstein, G. Application of texture analysis for optimizing thermo-mechanical treatment of a high Mn TWIP steel. *Adv. Mater. Res.* **2014**, *922*, 213–218. [CrossRef]
46. Wu, D.; Meng, C.; Mao, W.; Ou, X.; Song, M. Microstructural Evolution and Tensile Performance of a Commercial Fe–Mn–Al–C High-Manganese Steel. *Steel Res. Int.* **2023**, *94*, 2200877. [CrossRef]

47. Powell, D.J.; Pilkington, R.; Miller, D.A. The precipitation characteristics of 20% Cr/25% Ni-Nb stabilised stainless steel. *Acta Metall.* **1988**, *36*, 713–724. [CrossRef]
48. Wang, M.; Sun, H.; Phaniraj, M.P.; Han, H.N.; Jang, J.; Zhou, Z. Evolution of microstructure and tensile properties of Fe-18Ni-12Cr based AFA steel during aging at 700 °C. *Mater. Sci. Eng. A* **2016**, *672*, 23–31. [CrossRef]

Disclaimer/Publisher's Note: The statements, opinions and data contained in all publications are solely those of the individual author(s) and contributor(s) and not of MDPI and/or the editor(s). MDPI and/or the editor(s) disclaim responsibility for any injury to people or property resulting from any ideas, methods, instructions or products referred to in the content.